Performance Analysis of Matched-Filter Precoded MISO-OFDM Systems in the Presence of Imperfect CSI

Trung-Hien Nguyen[1], Jérôme Louveaux[2], Philippe De Doncker[1], and François Horlin[1]
[1]OPERA department, Université libre de Bruxelles (ULB), 1050 Brussels, Belgium
[2]ICTEAM institute, Université catholique de Louvain (UCL), 1348 Louvain-la-Neuve, Belgium
Email: trung-hien.nguyen@ulb.ac.be

***Abstract*—Multiple-antenna technologies provide a good spatial diversity gain for emerging communication systems. In combination to the orthogonal frequency division multiplexing (OFDM) modulation, a precoding system can be easily implemented and efficient to combat the effect of fading channels. However, the precoding system requires a perfect knowledge of the channel, which is not usually hold in practical cases. In this paper, we investigate the impact of the imperfect channel state information (CSI) on the downlink performance of multiple-input single-output (MISO) OFDM systems using a matched-filter (MF) precoder. Particularly, the exact mean-square-error (MSE) expression of the equalized received signal of the MF precoding system is derived. Numerical simulations with Rayleigh fading channels are carried out to validate the analysis. The results show that the imperfect CSI-based precoder causes a MSE plateau compared to the ideal case of using the perfect CSI.**

***Index terms*—** MF, MISO, OFDM, imperfect CSI.

I. Introduction

Massive multiple-input multiple-output (MIMO) antenna systems are now widely considered as enabling technologies for 5G communication systems [1]. It has been shown that a good spatial diversity and array gains can be achieved when combining with precoding techniques such as matched-filter (MF) [2] or maximum-ratio-transmission (MRT) [3]. Massive MIMO systems can operate in either time-division duplexing (TDD) or frequency-division duplexing (FDD) modes [4]. However, the FDD massive MIMO system requires a dedicated feedback channel for the channel state information (CSI)-based precoding with a large amount of pilots (proportional to the number of base-station antennas), which is also sensitive to the feedback delays [5]. The TDD massive MIMO system, requiring less overhead than the FDD one, exploits the channel reciprocity and uses the uplink CSIs for the downlink precoding. However, the time delay between the uplink CSI estimation and the downlink CSI-based precoding transmission may be bigger than the coherence time of the channel, making the CSI-based precoding imperfect [6].

It is well known that precoding techniques can easily be implemented in orthogonal frequency-division multiplexing (OFDM) systems, to efficiently combat the channel frequency selectivity [7]. Although both MRT and MF precoding techniques simplify the signal processing at the receiver side, the MF precoder is particularly interesting compared to the MRT one because of the simple pre-processing of the transmitted signals [8]. For instance, it is shown that in the multiple-input single-output (MISO) OFDM system, the MF precoding does not require the channel information exchange among antennas as the MRT precoding does [8], making it easy to implement in geographically distributed MISO systems. In a rich scattering environment, the MF precoding provides a significant focusing gain [9].

Because of the interest of using the MF precoding, the performance analysis of the MF precoding systems plays an important role to gain insights in system performance evaluation and to avoid the lengthy simulations. An analysis of the average bit-error-ratio (BER) of the MF precoded MISO-OFDM system has been carried out in [8]. However, the system was assumed to be perfectly synchronized and the CSI was also assumed to be perfect. Recently, the mean-square-error (MSE) analysis of the impact of carrier frequency offset (CFO) on the MF precoded MISO-OFDM system has been investigated [10]. However, the perfect CSI was again assumed. In practice, due to feedback delays and the fast time-varying nature of the fading channels, the perfect CSI assumption is not valid. In this paper, we investigate the impact of the outdated CSI used for MF precoding in MISO OFDM systems, which can be applied for any number of the transmit antennas. More specifically, our contributions are summarized as (1) the derivation of the exact closed-form MSE expression of the received equalized signal in MF precoded MISO-OFDM systems; (2) the asymptotic MSE analysis to show the reason of MSE plateau caused by the imperfect CSI-based precoding; (3) numerical simulations to validate the derived formulas.

Notation: Bold lower-case and upper-case letters denote column vectors and matrices, respectively; $\mathbf{I}_Q$, $\mathbf{F}_Q$ are the $Q \times Q$ identity and Fourier matrices, respectively;

$\mathbf{\Lambda_x}$ is the diagonal matrix whose diagonal entries are the elements of the vector $\mathbf{x}$; $\mathrm{tr}\{\mathbf{A}\}$ is the trace of a square matrix $\mathbf{A}$; $\Gamma(x)$ is the Gamma function; $||\cdot||$, $(\cdot)^*$, $(\cdot)^H$, $(\cdot)^T$, and $\mathbb{E}[\cdot]$ are the Euclidean norm, complex conjugate, Hermitian transpose, transpose and expectation operators, respectively.

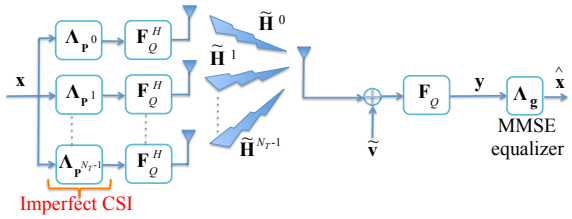

Fig. 1. A schematic of MF precoded MISO-OFDM system.

II. MF Precoded MISO-OFDM Systems

We consider a downlink $N_T \times 1$ MISO OFDM system (Fig. 1). We assume that the CSIs between each transmit antenna and the receive antenna are used at both transmitter (Tx) and receiver (Rx). Unfortunately, due to the feedback delays of the channel estimation from the receiver to the transmitter side, the MF precoding is imperfect. In order to focus on the impact of the imperfect CSI, we assume that the system synchronization is perfect. Furthermore, only one size-Q OFDM symbol transmission is considered for simplicity, $\mathbf{x} = [X_0 \ ... \ X_{Q-1}]^T$ (X_q is an independent zero-mean random variable (RV) with variance $\mathbb{E}[|X_q|^2] = \sigma_X^2$). This OFDM symbol is then precoded by a matrix $\mathbf{\Lambda_{p}}^k$ on each antenna branch k. We define $\mathbf{h}^k \triangleq [H_0^k \ H_1^k \ ... \ H_{Q-1}^k]^T$ as the channel frequency response (CFR) associated with the k-th antenna. Vector $\mathbf{p}^k \triangleq [P_0^k \ P_1^k \ ... \ P_{Q-1}^k]^T$ stacks the precoding values of associated CFR between the k-th Tx antenna and the Rx antenna. The precoding vector are usually normalized to unity. Particularly, at the q-th subcarrier and the k-th antenna, the MF precoding with imperfect CFR is $P_q^k = \left(\rho\left(H_q^k\right)^* + \sqrt{1-\rho^2}\left(n_q^k\right)^*\right) \Big/ \sqrt{N_T}$, where $\rho \in [0,1]$ represents the amount of the imperfection of CFR, n_q^k is assumed to be the zero-mean circularly complex Gaussian RV, i.e., $n_q^k \sim \mathcal{CN}(0,1)$, to facilitate the analysis. It reduces to $P_q^k = \left(H_q^k\right)^* \Big/ \sqrt{N_T}$, when the CFR knowledge is perfect. Hence, the precoding vector is represented as $\mathbf{p}^k = \left(\rho \cdot \mathbf{h}^k + \sqrt{1-\rho^2} \cdot \mathbf{n}^k\right)^* \Big/ \sqrt{N_T}$. The signals are then transformed to the time domain. The signal is then made cyclic by adding the cyclic prefix (CP) and propagated over the channel, which is mathematically equivalent to the left multiplication with the $Q \times Q$ circulant matrix $\widetilde{\mathbf{H}}^k$ of the k-th CSI. We assume that the CSIs between each transmit antenna and receive antenna are spatially independent from one to another. The matrix $\widetilde{\mathbf{H}}^k$ can be factorized as $\widetilde{\mathbf{H}}^k = \mathbf{F}_Q^H \cdot \mathbf{\Lambda_h}^k \cdot \mathbf{F}_Q$.

At the receiver side, the received signals are corrupted by the additive white Gaussian noise (AWGN) $\widetilde{\mathbf{v}}$. The signals are brought back to the frequency domain (FD) after CP removal by a fast Fourier transform (FFT) and can be expressed as $\mathbf{y} = \mathbf{F}_Q \cdot \left(\sum_{k=0}^{N_T-1} \widetilde{\mathbf{H}}^k \mathbf{F}_Q^H \mathbf{\Lambda_p}^k\right) \cdot \mathbf{x} + \mathbf{v} = \left(\sum_{k=0}^{N_T-1} \mathbf{\Lambda_h}^k \mathbf{\Lambda_p}^k\right) \cdot \mathbf{x} + \mathbf{v}$, where $\mathbf{v} = \mathbf{F}_Q \cdot \widetilde{\mathbf{v}} = [V_0, V_1, ..., V_{Q-1}]^T$ is the FD AWGN of variance $\mathbb{E}[|V_q|^2] = \sigma_V^2$. Since all the matrices are diagonal, the received signal $\mathbf{y}$ can be rewritten as

$$\mathbf{y} = \rho \mathbf{\Lambda_k} \cdot \mathbf{x} + \sqrt{1-\rho^2}\mathbf{\Lambda_c} \cdot \mathbf{x} + \mathbf{v}, \tag{1}$$

where $\mathbf{k} = [K_0, K_1, ..., K_{Q-1}]^T$ stacks q-th component defined as $K_q \triangleq \left(1/\sqrt{N_T}\right) \sum_{k=0}^{N_T-1} \left|H_q^k\right|^2$. Vector $\mathbf{c} = [c_0, c_1, ..., c_{Q-1}]^T$ represents the additional term caused by imperfect CSI-based precoding, in which the q-th component is defined as $c_q \triangleq \left(1/\sqrt{N_T}\right) \sum_{k=0}^{N_T-1} H_q^k (n_q^k)^*$.

Considering a minimum-mean-square-error (MMSE) equalizer $\mathbf{\Lambda_g}$, the estimated symbol can be expressed as $\widehat{\mathbf{x}} = \mathbf{\Lambda_g} \cdot \mathbf{y}$, where $\mathbf{g} = \left[\frac{K_0}{K_0^2+\gamma^{-1}}, ..., \frac{K_{Q-1}}{K_{Q-1}^2+\gamma^{-1}}\right]^T$ and $\gamma \triangleq \sigma_X^2/\sigma_V^2$ is the signal-to-noise ratio (SNR). In the case of perfect CSI-based precoding, i.e., $\rho = 1$, the received signal becomes $\widehat{\mathbf{x}} = \mathbf{\Lambda_g} \cdot \mathbf{\Lambda_k} \cdot \mathbf{x} + \mathbf{\Lambda_g} \cdot \mathbf{v}$. Note that, thanks to the precoding, the equalizer coefficients are real-valued, which brings a receiver complexity reduction.

III. Performance Analysis

A. MSE Derivation

We define the equalized symbol error as $\mathbf{e} \triangleq \widehat{\mathbf{x}} - \mathbf{x}$, the MSE is then calculated by $MSE = \mathbb{E}\left[\mathbf{e}^H \cdot \mathbf{e}\right] = \mathbb{E}\left[\mathrm{tr}\left\{\mathbf{e} \cdot \mathbf{e}^H\right\}\right]$. We further define the normalized MSE (NMSE) as $NMSE \triangleq MSE/\left(Q\sigma_X^2\right)$. Due to the fact that $\mathbb{E}[X_q V_q] = 0$, $\mathbb{E}[n_q^k] = 0$, after some manipulations, we obtain

$$\begin{aligned} NMSE = 1 &+ \frac{\rho^2}{Q}\mathrm{tr}\left\{\mathbb{E}\left[\mathbf{\Lambda_g}\mathbf{\Lambda_k}\mathbf{\Lambda_k}^H\mathbf{\Lambda_g}^H\right]\right\} \\ &+ \frac{\gamma^{-1}}{Q}\mathrm{tr}\left\{\mathbb{E}\left[\mathbf{\Lambda_g}^2\right]\right\} - \frac{2\rho}{Q}\mathrm{tr}\left\{\mathbb{E}\left[\mathbf{\Lambda_g}\mathbf{\Lambda_k}\right]\right\} \\ &+ \frac{(1-\rho^2)}{Q}\mathrm{tr}\left\{\mathbb{E}\left[\mathbf{\Lambda_g}\mathbf{\Lambda_c}\mathbf{\Lambda_c}^H\mathbf{\Lambda_g}^H\right]\right\}. \end{aligned} \tag{2}$$

We define $\left(\sigma_l^k\right)^2 \triangleq \mathbb{E}\left[\left|h_l^k\right|^2\right]$ as the variance of l-th tap of the k-th CSI between the k-th transmit antenna and the receive antenna. We assume that each tap of the CSI is independent (i.e., constructed from the uncorrelated scattering) and follows the Rayleigh fading channel distribution. As a consequence, the corresponding CFR components H_q^k are independently and identically distributed (i.i.d.). Based on the derivation made in

Appendix, the exact closed-form NMSE expression (3) is obtained, where S_{1n}, S_{2n} and S_{4n} ($n \in \{1, 2, 3, 4\}$) are defined in equations from (11) to (22), containing only the elementary functions.

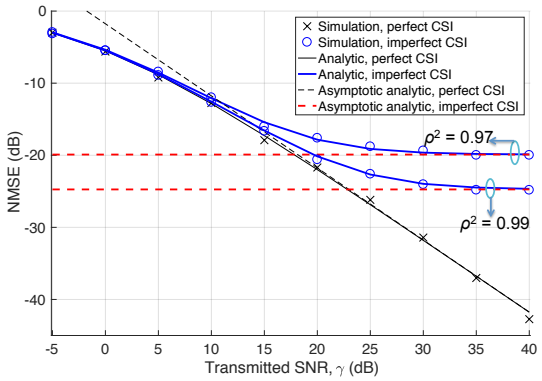

Fig. 2. NMSE versus SNRs in MF precoded 4×1 MISO system.

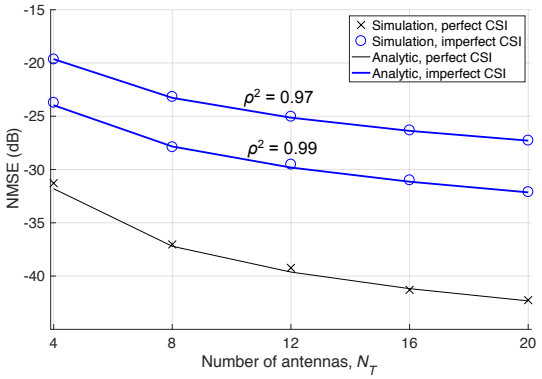

Fig. 3. NMSE versus the number of antennas when SNR = 30 dB.

From the derived NMSE expression, the NMSE can be split into two parts. The first one is equal to the case of using the perfect CSI, referred to as $NMSE_{perfect}$ (4), while the second one corresponds to the contribution of the imperfect CSI, called $NMSE_{impefect}$ (5), such that $NMSE_{perfect} + NMSE_{imperfect} = NMSE$. To gain insights in the negative contribution on MSE performance when using the imperfect CSI-based precoding, we study the asymptotic MSE at high SNRs in the following section.

B. Asymptotic MSE Analysis

At high SNRs, we first notice that the MMSE equalizer reduces to the ZF equalizer, meaning that $\mathbf{\Lambda_g} = \mathbf{\Lambda_k}^{-1}$. Therefore, the NMSE of using perfect CSI at high SNRs, $NMSE^{high}_{perfect}$, is readily derived as

$$NMSE^{high}_{perfect} = \frac{\gamma^{-1}}{Q}\mathrm{tr}\left\{\mathbb{E}\left[\mathbf{\Lambda_g^2}\right]\right\} = \frac{-T_2}{4\Gamma\left(N_T\right)} \overset{N_T \geq 2}{\rightarrow} \frac{\gamma^{-1} N_T}{\left(N_T - 1\right)\left(N_T - 2\right)} \quad (6)$$

where we use the fact that when the perfect CSI is used, $\rho = 1$, based on (2), it is easy to show that $1 + \frac{1}{Q}\mathrm{tr}\left\{\mathbb{E}\left[\mathbf{\Lambda_g \Lambda_k \Lambda_k^H \Lambda_g^H}\right]\right\} - \frac{2}{Q}\mathrm{tr}\left\{\mathbb{E}\left[\mathbf{\Lambda_g \Lambda_k}\right]\right\} = 0$.

When precoding the signal by the imperfect CSI, from (2) the additional NMSE at high SNRs, $NMSE^{high}_{imperfect}$, is rewritten as

$$NMSE^{high}_{imperfect} = 1 + \rho^2 - 2\rho + \frac{\left(1 - \rho^2\right)}{Q}\mathrm{tr}\left\{\mathbb{E}\left[\mathbf{\Lambda_g \Lambda_c \Lambda_c^H \Lambda_g^H}\right]\right\} \overset{N_T \geq 1}{\rightarrow} \left(1 - \rho\right)^2 + \frac{1 - \rho^2}{N_T - 1}. \quad (7)$$

Since $(1 - \rho)^2 \geq 0$ and $1 - \rho^2 \geq 0$, it is obvious that $NMSE^{high}_{imperfect} \geq 0$, meaning that the imperfect CSI used for precoding causes a plateau for the NMSE, leading to the performance degradation (the detailed asymptotic derivations are omitted due to the space constraint). The NMSE plateau can be reduced by increasing the number of antennas. In what follows, we numerically validate the derived formulas.

IV. Results and Discussion

A multi-path channel of type Extended Pedestrian A (EPA) [11] with a power delay profile (PDP) detailed in [2] is used in simulations. The overall channel power is normalized to unity. Each channel tap is assumed to be statistically independent. We consider a 256-subcarrier MISO OFDM system. In order to focus on the impact of the imperfect CSI-based precoding, the synchronization at the receiver side is assumed to be perfect. The numerical and analytical results are presented by the marker symbols and solid (or dashed) lines, respectively.

We present in Fig. 2 the NMSE as a function of the SNR for the 4×1 MISO OFDM system, when the imperfect CSI-based precoding is applied with $\rho^2 = 0.97$ and $\rho^2 = 0.99$. It is clearly seen that the imperfect CSI-based precoding causes a MSE plateau at high SNRs, i.e., SNR > 30 dB. The asymptotic MSE formulas derived in (6) and (7) are also plotted. All the numerical results match the analytical ones, confirming the correctness of our derivations. Fig. 3 presents the NMSE as a function of the number of antennas, showing that in the presence of the imperfect CSI, the NMSE can be reduced by increasing the number of antennas.

V. Conclusion

We have studied the impact of imperfect CSI on the MF precoded MISO-OFDM system. By considering Rayleigh fading channels, we have derived the exact closed-form MSE expression of the received equalized symbols. The MSE converges to a plateau when the precoder is built based on the imperfect CSI. The plateau can be reduced by increasing the number of antennas. The correctness of the analytical derivation has been numerically confirmed.

$$NMSE = 1 - \frac{\rho^2}{4N_T\gamma^{-1}\Gamma\left(N_T\right)} \cdot T_1 - \frac{1}{4\Gamma\left(N_T\right)} \cdot T_2 - \frac{\rho}{j(N_T\gamma^{-1})^{1/2}\Gamma\left(N_T\right)} \cdot T_3 - \frac{1-\rho^2}{4N_T\gamma^{-1}\Gamma\left(N_T\right)} \cdot T_4.$$

$$T_1 = \mathrm{e}^{-j\left(N_T\gamma^{-1}\right)^{1/2}} S_{11} + \mathrm{e}^{j\left(N_T\gamma^{-1}\right)^{1/2}} S_{12} - \frac{\mathrm{e}^{-j\left(N_T\gamma^{-1}\right)^{1/2}}}{j(N_T\gamma^{-1})^{1/2}} S_{13} + \frac{\mathrm{e}^{j\left(N_T\gamma^{-1}\right)^{1/2}}}{j(N_T\gamma^{-1})^{1/2}} S_{14}.$$

$$T_2 = \mathrm{e}^{-j\left(N_T\gamma^{-1}\right)^{1/2}} S_{21} + \mathrm{e}^{j\left(N_T\gamma^{-1}\right)^{1/2}} S_{22} - \frac{\mathrm{e}^{-j\left(N_T\gamma^{-1}\right)^{1/2}}}{j(N_T\gamma^{-1})^{1/2}} S_{23} + \frac{\mathrm{e}^{j\left(N_T\gamma^{-1}\right)^{1/2}}}{j(N_T\gamma^{-1})^{1/2}} S_{24}.$$

$$T_3 = \mathrm{e}^{-j\left(N_T\gamma^{-1}\right)^{1/2}} S_{23} - \mathrm{e}^{j\left(N_T\gamma^{-1}\right)^{1/2}} S_{24}.$$

$$T_4 = \mathrm{e}^{-j\left(N_T\gamma^{-1}\right)^{1/2}} S_{41} + \mathrm{e}^{j\left(N_T\gamma^{-1}\right)^{1/2}} S_{42} - \frac{\mathrm{e}^{-j\left(N_T\gamma^{-1}\right)^{1/2}}}{j(N_T\gamma^{-1})^{1/2}} S_{43} + \frac{\mathrm{e}^{j\left(N_T\gamma^{-1}\right)^{1/2}}}{j(N_T\gamma^{-1})^{1/2}} S_{44}. \quad (3)$$

$$NMSE_{perfect} = 1 - \frac{T_1}{4N_T\gamma^{-1}\Gamma\left(N_T\right)} - \frac{T_2}{4\Gamma\left(N_T\right)} - \frac{T_3}{j(N_T\gamma^{-1})^{1/2}\Gamma\left(N_T\right)}. \quad (4)$$

$$NMSE_{imperfect} = \frac{\left(1-\rho^2\right)\left(T_1 - T_4\right)}{4N_T\gamma^{-1}\Gamma\left(N_T\right)} + \frac{\left(1-\rho\right)T_3}{j(N_T\gamma^{-1})^{1/2}\Gamma\left(N_T\right)}. \quad (5)$$

APPENDIX

The RV $R_q = \sum_{k=0}^{N_T-1} \left|H_q^k\right|^2$ has a probability density function (PDF) $f_R\left(r\right) = \frac{r^{N_T-1}\mathrm{e}^{-r}}{(N_T-1)!}$ [12]. We first derive the second term on the right-hand-side (RHS) of (2) $E_1 = \frac{\rho^2}{Q}\mathrm{tr}\left\{\mathbb{E}\left[\mathbf{\Lambda_g}\mathbf{\Lambda_k}\mathbf{\Lambda_k}^H\mathbf{\Lambda_g}^H\right]\right\}$. It can be rewritten as

$$E_1 = \rho^2\mathbb{E}\left[\frac{R_q^4}{\left(R_q^2 + N_T\gamma^{-1}\right)^2}\right] = \frac{\rho^2}{\Gamma\left(N_T\right)}\int_0^\infty \frac{r^{N_T+3}}{\left(r^2+N_T\gamma^{-1}\right)^2}\mathrm{e}^{-r}dr. \quad (8)$$

The key derivation is based on the fraction decomposition $\frac{r^{N_T+3}}{(r^2+N_T\gamma^{-1})^2} = \frac{-r^{N_T+3}}{4N_T\gamma^{-1}}\left(\frac{1}{\left(r-j(N_T\gamma^{-1})^{1/2}\right)^2} + \frac{1}{\left(r+j(N_T\gamma^{-1})^{1/2}\right)^2} - \frac{1/\left(j\left(N_T\gamma^{-1}\right)^{1/2}\right)}{r-j(N_T\gamma^{-1})^{1/2}} + \frac{1/\left(j\left(N_T\gamma^{-1}\right)^{1/2}\right)}{r+j(N_T\gamma^{-1})^{1/2}}\right)$.
Hence, E_1 is decomposed into $E_1 = \frac{-\rho^2}{4N_T\gamma^{-1}\Gamma(N_T)}\left(E_{11} + E_{12} - \frac{E_{13}}{j(N_T\gamma^{-1})^{1/2}} + \frac{E_{14}}{j(N_T\gamma^{-1})^{1/2}}\right)$, in which the integral E_{11} is computed as follows

$$E_{11} = \int_0^\infty \frac{r^{N_T+3}}{\left(r - j(N_T\gamma^{-1})^{1/2}\right)^2}\mathrm{e}^{-r}dr \overset{(1)}{=} \int_{j(N_T\gamma^{-1})^{1/2}}^\infty \frac{\left(t + j\left(N_T\gamma^{-1}\right)^{1/2}\right)^{N_T+3}}{\mathrm{e}^{j(N_T\gamma^{-1})^{1/2}}t^2}\mathrm{e}^{-t}dt \overset{(2)}{=} \mathrm{e}^{-j\left(N_T\gamma^{-1}\right)^{1/2}} S_{11}, \quad (9)$$

where the equality (1) is reached by making a variable change $t = r - j\left(N_T\gamma^{-1}\right)^{1/2}$, the equality (2) makes use of the binomial formula $(x+y)^n = \sum_{k=0}^{n}\left(\begin{array}{c} n \\ k \end{array}\right)x^k y^{n-k}$. Term S_{11} is presented in (11), in which the upper incomplete Gamma function $\Gamma_{up}(\eta, z)$ is defined as $\Gamma_{up}\left(\eta, z\right) \triangleq \int_z^\infty t^{\eta-1}\mathrm{e}^{-t}dt$. Similarly, the integrals E_{12}, E_{13} and E_{14} are derived as

$$E_{12} = \int_0^\infty \frac{r^{N_T+3}\mathrm{e}^{-r}dr}{\left(r + j(N_T\gamma^{-1})^{1/2}\right)^2} = \mathrm{e}^{j\left(N_T\gamma^{-1}\right)^{1/2}} S_{12}.$$

$$E_{13} = \int_0^\infty \frac{r^{N_T+3}\mathrm{e}^{-r}dr}{r - j(N_T\gamma^{-1})^{1/2}} = \mathrm{e}^{-j\left(N_T\gamma^{-1}\right)^{1/2}} S_{13}.$$

$$E_{14} = \int_0^\infty \frac{r^{N_T+3}\mathrm{e}^{-r}dr}{r + j(N_T\gamma^{-1})^{1/2}} = \mathrm{e}^{j\left(N_T\gamma^{-1}\right)^{1/2}} S_{14}, \quad (10)$$

where S_{12}, S_{13} and S_{14} are shown in (12), (13) and (14), respectively.

On the RHS of (2), the third term $E_2 = \frac{\gamma^{-1}}{Q}\mathrm{tr}\left\{\mathbb{E}\left[\mathbf{\Lambda_g}^2\right]\right\} = \frac{\gamma^{-1}N_T}{\Gamma(N_T)}\int_0^\infty \frac{r^{N_T+1}}{(r^2+N_T\gamma^{-1})^2}\mathrm{e}^{-r}dr$, the fourth term $E_3 = \frac{2\rho}{Q}\mathrm{tr}\left\{\mathbb{E}\left[\mathbf{\Lambda_g}\mathbf{\Lambda_k}\right]\right\} = \frac{2\rho}{\Gamma(N_T)}\int_0^\infty \frac{r^{N_T+1}}{r^2+N_T\gamma^{-1}}\mathrm{e}^{-r}dr$ and the fifth term $E_4 = \frac{\left(1-\rho^2\right)}{Q}\mathrm{tr}\left\{\mathbb{E}\left[\mathbf{\Lambda_g}\mathbf{\Lambda_c}\mathbf{\Lambda_c}^H\mathbf{\Lambda_g}^H\right]\right\} = \frac{1-\rho^2}{\Gamma(N_T)}\int_0^\infty \frac{r^{N_T+2}}{(r^2+N_T\gamma^{-1})^2}\mathrm{e}^{-r}dr$ can be derived similar to E_1 derivation, but they are skipped due to the space constraint. Finally, substituting E_1, E_2, E_3 and E_4 into (2), we obtain (3).

$$S_{11} = \sum_{k=0}^{N_T+3} \left(\begin{array}{c} N_T+3 \\ k \end{array} \right) \Gamma_{up} \left(k-1, -j\left(N_T\gamma^{-1}\right)^{1/2} \right) \left(j\left(N_T\gamma^{-1}\right)^{1/2} \right)^{N_T+3-k}. \quad (11)$$

$$S_{12} = \sum_{k=0}^{N_T+3} \left(\begin{array}{c} N_T+3 \\ k \end{array} \right) \Gamma_{up} \left(k-1, j\left(N_T\gamma^{-1}\right)^{1/2} \right) \left(-j\left(N_T\gamma^{-1}\right)^{1/2} \right)^{N_T+3-k}. \quad (12)$$

$$S_{13} = \sum_{k=0}^{N_T+3} \left(\begin{array}{c} N_T+3 \\ k \end{array} \right) \Gamma_{up} \left(k, -j\left(N_T\gamma^{-1}\right)^{1/2} \right) \left(j\left(N_T\gamma^{-1}\right)^{1/2} \right)^{N_T+3-k}. \quad (13)$$

$$S_{14} = \sum_{k=0}^{N_T+3} \left(\begin{array}{c} N_T+3 \\ k \end{array} \right) \Gamma_{up} \left(k, j\left(N_T\gamma^{-1}\right)^{1/2} \right) \left(-j\left(N_T\gamma^{-1}\right)^{1/2} \right)^{N_T+3-k}. \quad (14)$$

$$S_{21} = \sum_{k=0}^{N_T+1} \left(\begin{array}{c} N_T+1 \\ k \end{array} \right) \Gamma_{up} \left(k-1, -j\left(N_T\gamma^{-1}\right)^{1/2} \right) \left(j\left(N_T\gamma^{-1}\right)^{1/2} \right)^{N_T+1-k}. \quad (15)$$

$$S_{22} = \sum_{k=0}^{N_T+1} \left(\begin{array}{c} N_T+1 \\ k \end{array} \right) \Gamma_{up} \left(k-1, j\left(N_T\gamma^{-1}\right)^{1/2} \right) \left(-j\left(N_T\gamma^{-1}\right)^{1/2} \right)^{N_T+1-k}. \quad (16)$$

$$S_{23} = \sum_{k=0}^{N_T+1} \left(\begin{array}{c} N_T+1 \\ k \end{array} \right) \Gamma_{up} \left(k, -j\left(N_T\gamma^{-1}\right)^{1/2} \right) \left(j\left(N_T\gamma^{-1}\right)^{1/2} \right)^{N_T+1-k}. \quad (17)$$

$$S_{24} = \sum_{k=0}^{N_T+1} \left(\begin{array}{c} N_T+1 \\ k \end{array} \right) \Gamma_{up} \left(k, j\left(N_T\gamma^{-1}\right)^{1/2} \right) \left(-j\left(N_T\gamma^{-1}\right)^{1/2} \right)^{N_T+1-k}. \quad (18)$$

$$S_{41} = \sum_{k=0}^{N_T+2} \left(\begin{array}{c} N_T+2 \\ k \end{array} \right) \Gamma_{up} \left(k-1, -j\left(N_T\gamma^{-1}\right)^{1/2} \right) \left(j\left(N_T\gamma^{-1}\right)^{1/2} \right)^{N_T+2-k}. \quad (19)$$

$$S_{42} = \sum_{k=0}^{N_T+2} \left(\begin{array}{c} N_T+2 \\ k \end{array} \right) \Gamma_{up} \left(k-1, j\left(N_T\gamma^{-1}\right)^{1/2} \right) \left(-j\left(N_T\gamma^{-1}\right)^{1/2} \right)^{N_T+2-k}. \quad (20)$$

$$S_{43} = \sum_{k=0}^{N_T+2} \left(\begin{array}{c} N_T+2 \\ k \end{array} \right) \Gamma_{up} \left(k, -j\left(N_T\gamma^{-1}\right)^{1/2} \right) \left(j\left(N_T\gamma^{-1}\right)^{1/2} \right)^{N_T+2-k}. \quad (21)$$

$$S_{44} = \sum_{k=0}^{N_T+2} \left(\begin{array}{c} N_T+2 \\ k \end{array} \right) \Gamma_{up} \left(k, j\left(N_T\gamma^{-1}\right)^{1/2} \right) \left(-j\left(N_T\gamma^{-1}\right)^{1/2} \right)^{N_T+2-k}. \quad (22)$$

ACKNOWLEDGMENT

The authors would like to thank the financial supports of the Copine-IoT Innoviris project, the Icity.Brussels project and the FEDER/EFRO grant.

REFERENCES

[1] H. Q. Ngo, E. G. Larsson, and T. L. Marzetta, "Energy and spectral efficiency of very large multiuser MIMO systems," IEEE Trans. Commun., vol. 61, no. 4, pp. 1436–1449, Apr. 2013.

[2] T.-H. Nguyen, J.-F. Determe, M. Van Eeckhaute, J. Louveaux, P. De Doncker, and F. Horlin, "Frequency-domain time-reversal precoding in wideband MISO OFDM communication systems," 2019. [Online] Available: https://arxiv.org/abs/1904.10727.

[3] T. K. Y. Lo, "Maximum ratio transmission," IEEE Trans. Commun., vol. 47, no. 10, pp. 1458–1461, Oct. 1999.

[4] T. L. Marzetta, "Noncooperative cellular wireless with unlimited numbers of base station antennas," IEEE Trans. Wireless Commun., vol. 9, no. 11, pp. 3590–3600, Nov. 2010.

[5] J. Choi, D. Love, and P. Bidigare, "Downlink training techniques for FDD massive MIMO systems: Open-loop and closed-loop training with memory," IEEE J. Sel. Topics Signal Process., vol. 8, no. 5, pp. 802–814, Oct. 2014.

[6] E. Bjornson, J. Hoydis, M. Kountouris, and M. Debbah, "Massive MIMO systems with non-ideal hardware: Energy efficiency, estimation, and capacity limits," IEEE Trans. Inf. Theory, vol. 60, no. 11, pp. 7112–7139, Nov. 2014.

[7] M. Speth, S. Fechtel, G. Fock, and H. Meyr, "Optimum receiver design for wireless broad-band systems using OFDM - Part I," IEEE Trans. Commun., vol. 47, no. 11, pp. 1668–1677, Nov. 1999.

[8] M. Maaz, M. Helard, P. Mary and M. Liu, "Performance analysis of time-reversal based precoding schemes in MISO-OFDM systems," Proc. IEEE 81st VTC Spring, May 2015.

[9] C. Oestges, A. Kim, G. Papanicolaou, and A. Paulraj, "Characterization of space-time focusing in time-reversed random fields," IEEE Trans. Antennas Propag., vol. 53, no. 1, pp. 283–293, Jan. 2005.

[10] T.-H. Nguyen, M. Van Eeckhaute, J.-F. Determe, J. Louveaux, P. De Doncker, and F. Horlin, "Analysis of residual CFO impact on downlink massive MISO systems," IET Electron. Lett., vol. 55, no. 18, pp. 1017–1019, Sep. 2019.

[11] 3GPP - TS 36.101, "User Equipment (UE) Radio Transmission and Reception." 3rd Generation Partnership Project; Technical Specification Group Radio Access Network; Evolved Universal Terrestrial Radio Access (E-UTRA). URL: http://www.3gpp.org.

[12] A. Papoulis, "Probability, random variables and stochastic processes," McGraw-Hill Companies, 3rd edition, 1991.